COMMUNICATIONS

Magnetic Resonance in Medicine 45:935–939 (2001)

Anisotropy in High Angular Resolution Diffusion-Weighted MRI

Lawrence R. Frank*

The diffusion in voxels with multidirectional fibers can be quite complicated and not necessarily well characterized by the standard diffusion tensor model. High angular resolution diffusion-weighted acquisitions have recently been proposed as a method to investigate such voxels, but the reconstruction methods proposed require sophisticated estimation schemes. We present here a simple algorithm for the identification of diffusion anisotropy based upon the variance of the estimated apparent diffusion coefficient (ADC) as a function of measurement direction. The rationale for this method is discussed, and results in normal human subjects acquired with a novel diffusion-weighted stimulated-echo spiral acquisition are presented which distinguish areas of anisotropy that are not apparent in the relative anisotropy maps derived from the standard diffusion tensor model. Magn Reson Med 45:935–939, 2001. Published 2001 Wiley-Liss, Inc.†

Key words: diffusion; anisotropy; spherical diffusion variance; high angular resolution; white matter

The sensitivity of NMR to diffusion (1) has long been exploited as a method for investigating molecular motions in complex systems by measurement of the diffusion coefficient (2–5). The recognition that NMR can be made sensitive to the details of anisotropic diffusion in structured materials led to a formulation of the problem in which the diffusion is modeled as a tensor (6,7), rather than a scalar, as would be appropriate for a heterogenous system with Gaussian diffusion. This technique has been employed extensively in MRI to characterize regions of anisotropic tissues, such as white matter (8,9). More recently, this technique has been used as the basis for determining the orientation and connectivity of white matter fibers (e.g., Refs. 10–12), which holds great promise as an adjunct technique to functional MRI (fMRI) for mapping connections between functionally active regions.

A voxel with a single-fiber direction can be described by the diffusion tensor model, and therefore six measurements (in addition to a normalizing seventh) are sufficient to completely characterize the diffusion (6). Because the orientation of fibers is generally unknown, these measurements are typically acquired using diffusion-encoding gradient directions uniformly distributed on the surface of a sphere (13,14).

Department of Radiology, San Diego VA Healthcare System and University of California–San Diego, San Diego, California.

Grant sponsor: VA; Grant number: SA-321.

*Correspondence to: Lawrence R. Frank, Dept. of Radiology, San Diego VA Healthcare System and UC–San Diego, 3350 La Jolla Village Drive, 9114/MRI, San Diego, CA 92161.

Received 5 July 2000; revised 21 December 2000; accepted 5 February 2001.

However, a common situation in the imaging of fibrous biological systems, such as white matter, is the existence of multiple-fiber orientations within an imaging voxel, in which case the simple diffusion tensor model is inappropriate (6,13,15). While this problem can be reduced with higher-resolution acquisitions, voxels containing multiple-fiber orientations are likely whenever the imaging resolution is significantly larger than the fiber dimensions. The apparent diffusion coefficient (ADC) from such a voxel can have a complicated shape. However, a method for characterizing the diffusion from such a voxel, and a principle upon which to determine the optimal number of gradient directions required, have not yet been elucidated. However, a natural extension of the single-fiber case, proposed by Tuch et al. (16), is to acquire many gradient directions, still equally distributed on a sphere, but with angular resolution much higher than in the single-fiber case.

An important consideration in diffusion imaging of voxels with multiple fibers is the structure of the diffusion signal from a system with multiple compartments. The measured diffusion signal depends on the individual variances of each of the different compartments, so that the separability of the different components increases with increasing b-value. (The b-value incorporates the gradient strength and timing parameters that affect diffusion sensitivity through the relation of the signal attenuation $S(\boldsymbol{D})$ to the diffusion $\boldsymbol{D}$:$S(\boldsymbol{D}) \propto exp(-\boldsymbol{bD})$. See, for example Ref. 6).

The study by Tuch et al. (16) acquired high angular diffusion resolution images with large b-values, and extended the diffusion model to multiple-diffusion tensors within a voxel (16). This method of analysis requires an estimation scheme capable of constraining such an ill-posed problem to a reasonable solution (16). More recently, Wedeen et al. (17) suggested that the general inadequacy of the tensor model can be circumvented by adopting the viewpoint of Cory and Garroway (18) that diffusion sensitivity is generally a measure of the displacement probability distribution, in which case the Fourier transform of high angular resolution diffusion measurement data measured within a spherical volume can be seen as a measure of the distribution of fiber orientations.

In this work we point out that the shape of the surface of the measured diffusion along multiple directions for a single voxel in high angular resolution diffusion measurements can convey more information than the diffusion tensor. This idea leads to a very simple and practical method for the identification of diffusion anisotropy without the necessity of invoking the diffusion tensor formalism.

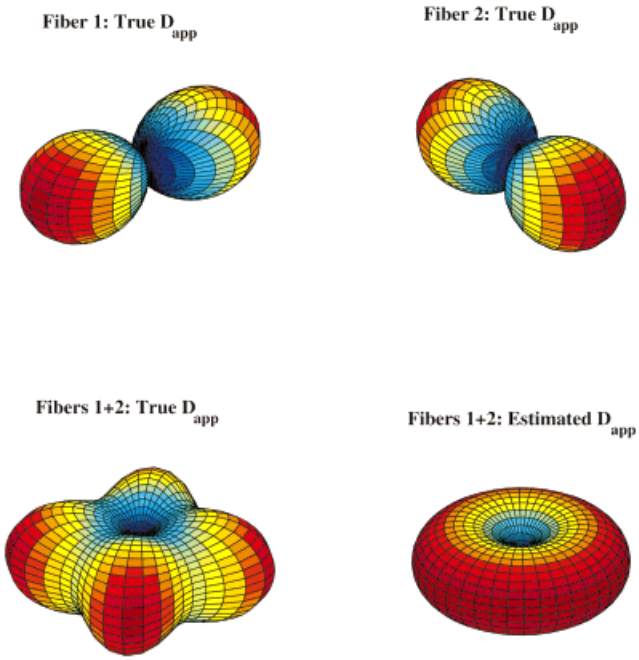

FIG. 1. Simulated ADC (D_{app}) as a function of the spherical coordinates (θ, ϕ) for two identical perpendicular cylindrically symmetric fibers with anisotropy ratio of 10:1:1 oriented 90° to one another. Top row: The D_{app} of each individual fiber (if they were isolated). Bottom row: (left) The true D_{app} for a voxel containing both fibers, and (right) the estimated D_{app} obtained from the standard diffusion tensor model. The color scales with D_{app}θ, ϕ) from blue (the lowest) to red (the highest).

THEORY

The measured diffusion coefficient along an arbitrary direction is proportional to the variance of the projection of the spin displacements (at the time of measurement) onto the measurement axis (19). Therefore, although the pattern of displacements of final spin positions is ellipsoidal, the *measured* quantity in a diffusion-weighted MR experiment is the *projection* of this ellipsoid onto the diffusion-sensitized axis, and it is the variance of this projection that gives the ADC D_{app}. Therefore the shape of D_{app} as a function of the measurement directions can be quite complicated. For example, if the diffusion is anisotropic and cylindrically symmetric, the ADC measured with gradient directions defined on the surface of a sphere and expressed as the radius from the origin as a function of the spherical coordinates (θ, ϕ) (the azimuthal and polar angles, respectively) has the shape of a peanut (Fig. 1 top).

In considering the case of crossed fibers, another property of the measured diffusion signal that becomes important is that it depends on the individual variances of each of the different compartments, so that the separability of the different components increases with increasing *b*-value. This can be seen from the signal equation from a voxel with two components with volume fractions α and β = 1 − α, respectively:

$$S = S_0(\alpha e^{-bD_{1,app}} + \beta e^{-bD_{2,app}}). \quad [1]$$

For small b, $S \approx S_0 e^{-b\bar{D}_{app}}$ where $\bar{D}_{app} \equiv \alpha D_{1,app} + \beta D_{2,app}$ is the weighted mean of the individual ADCs. In this case, $\log(S/S_0) \approx -b\bar{D}_{app}$ and a plot of $\log(S/S_0)$ vs. b is a straight line with a slope proportional to the mean ADC. However, for large b, this approximation cannot be made, and the form of $\log(S/S_0)$ becomes more complicated. This property of the diffusion signal is, in fact, quite important. Were the signal simply proportional to just the sum of the ADCs, separation of the individual compartments would not be possible.

As a function of (θ, ϕ), isotropic diffusion results in an ADC that is constant as a function of these angles and therefore forms a spherical surface. Anisotropic diffusion deviates from this spherical surface in a manner that depends upon the local diffusion. The deviation of the measurements from a spherical shape is therefore a measure of anisotropy. This does not depend on any characterization of the diffusion other than its deviation from a sphere. This is useful because although the surface due to diffusion along a single fiber is well characterized by the diffusion tensor, this is not necessarily so if there are multiple fibers within a voxel since the diffusion in this case can be quite complicated. However, it still possesses deviations from a spherical surface, even though the *shape* of these deviations is not well characterized.

This can be illustrated with a simple example, shown in Fig. 1, in which diffusion in a voxel containing two fibers is simulated. (Simulations were performed using MATLAB (Mathworks, Inc., Natick, MA). Two identical fibers are assumed to be coplanar and oriented relative to one another by an angle θ. The fibers are modeled, following Hsu and Mori (19), as cylindrically symmetric. The ratio of diffusion coefficients along the principle axes is 10:1:1, with the largest coplanar with the fibers. The maximum diffusion coefficient is taken to be that of white matter,

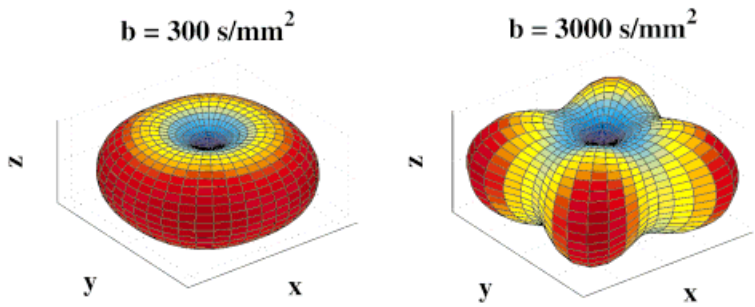

FIG. 2. Two-fiber diffusion at low and high *b*-values from crossed fibers with equal diffusion tensor components but oriented at 90° relative to one another. The diffusion tensor components are $D_1 = .75 * 10^{-3}$ mm^2/s, $D_2 = D_3 = D_1/10$. Distinction between the two fibers increases with increasing *b*-value. The separability of the diffusion compartments depends upon the magnitude of the *b*-values because the diffusion signal depends *independently* on the individual variances of each of the different compartments.

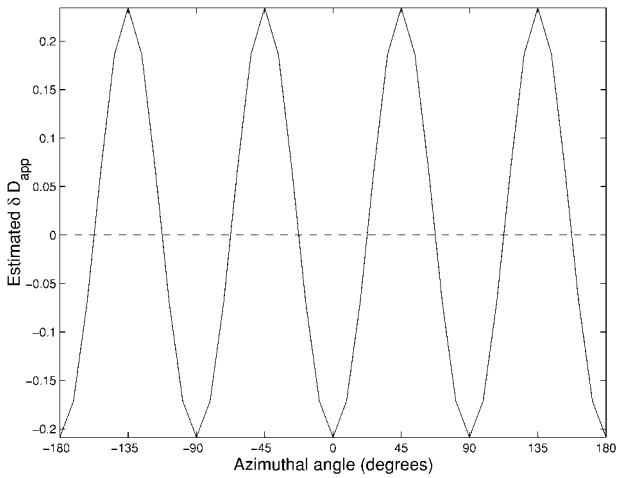

FIG. 3. Deviation about the azimuthal direction for the actual and the reconstructed ADC expressed as the variations from the mean: $\delta D_{app} \equiv (D_{app} - \bar{D}_{app})$.

$D = .75 \times 10^{-3}$ mm^2/s (13,15). The b-value is assumed to be $b = 3000$ s/mm^2. Shown in Fig. 1 are, from left to right, the ADC as a function of the spherical coordinates (θ, ϕ) for the two individual fibers (if they were in different voxels), the ADC from a voxel containing both fibers, and the estimated ADC that results from the diffusion tensor model. The separability of the individual diffusion compartments as a function of the b-value for two fibers is shown in a simulated voxel containing crossed fibers with equal diffusion tensor components, but oriented at 90° relative to one another (Fig. 2). It is readily apparent from Fig. 1 that although the actual diffusion possesses a significant amount of structure, the ADC estimated from the diffusion tensor model is completely symmetric in the $x - y$ plane, and therefore fails to reflect the inherent structure in the diffusion. This is emphasized in Fig. 3 by plotting the deviation about the azimuthal direction for the actual and the reconstructed ADC. This problem can be avoided by abandoning the diffusion tensor as the appropriate model for diffusion from which to derive a measure of anisotropy in favor of the variance of the measured ADCs: $\mathcal{V} \equiv var(D_{app}(\theta, \phi)) = \langle {D_{app}}^2 \rangle - \langle D_{app} \rangle^2$ where $D_{app} = -(1/b)\log(A(b, \theta, \phi)/A(b = 0))$ on the surface of the sphere defined by the gradient directions, computed from the measured signal amplitudes A along the different gradient directions. Here $\langle \cdot \rangle$ denotes the average over all measured gradient directions n: $(1/n) \sum_k^n D_{app,k}$. The data gives n measurements of D_{app} at n uniformly angularly-spaced directions, and the measure of anisotropy we propose is the variance of these measurements of D_{app}. This will be termed the *spherical diffusion variance* $\mathcal{V}$. This method avoids the problem of fitting an inappropriate model to the data, and allows the identification of regions of diffusion anisotropy.

METHODS

Images were acquired on a GE SIGNA 1.5T Clinical Imager with high-speed gradient hardware using a stimulated-echo sequence with a stimulated-echo spiral acquisition. Diffusion-sensitive images were acquired on five normal human subjects, with approval from the Human Subjects Committee at UC–San Diego. The spiral acquisition component was that designed by Glover (20), based on the work of Meyer et al. (21), optimized to acquire data at a maximum rate within the limits of gradient power and slew rate achievable by our scanner. Fat suppression was always employed.

The stimulated-echo spiral acquisition employed has not been previously described. Its utility in diffusion-weighted MRI stems from the marriage of the high-diffusion sensitizing capabilities of stimulated echoes with the motion insensitivity and acquisition speed of spiral acquisitions. Stimulated-echoes acquisitions are able to create large b-values, while limiting T_2 decay (22,23), because the diffusion sensitivity is proportional to the mixing time T_m between the second and third 90° pulse, during which the magnetization is longitudinal and not subject to T_2 decay. This has the added advantage that large diffusion sensitivities can be created for fixed gradient strength by varying the mixing time T_m, thereby reducing eddy current effects. The penalty paid is the signal diminution by a factor of 2 from the stimulated echo (22,23). Spiral acquisitions are advantageous in diffusion studies because they are relatively insensitive to motion (21), and their single-shot capability essentially eliminates motion during acquisitions while allowing reasonable scan times even with multiple diffusion angle encoding. Moreover, their facilitation of short echo times further reduces T_2 signal loss.

Following the procedure of Tuch et al. (16), high angular resolution diffusion encoding is achieved by generating gradient directions equally spaced on a sphere by tessellations of an icosahedron. This procedure produces directions that are equally separated in angle from one another so as to not bias measurements in any particular direction. The angular resolution (equivalently, the density of points on the spherical surface) is controlled by the tessellation level, which is input by the operator. The resulting gradient pattern is automatically generated by the pulse sequence. Results of this procedure (shown, for clarity, at a much higher degree of sampling) are shown in Fig. 4, in which the desired gradient sampling profile is shown on the left and the actual gradient directions computed by our pulse sequence are shown on the right. The numerical method for this has been implemented in a highly efficient manner that allows direct computation of many hundreds of gradient directions at scan time, without the need for storing large files of numbers, making the computations transparent to the user.

However, although spirals are relatively insensitive to motion, motion between scans can still degrade the quality of the diffusion data. In the present study, all images from a particular slice (i.e., all diffusion directions and averages at each direction) were registered using the image registration program IMREG from the AFNI suite of programs (24). The trade-off between the number of gradient directions acquired and the increased noise variance due to motion during the increased scanning time will be explored in future work. Single-shot imaging also significantly reduces scanning time, allowing the acquisition of many averages within a clinically reasonable time. In the present study, single-shot images were acquired at nine slices with the following parameters: FOV = 24 cm, slice thickness = 3.8 mm, and matrix size = 64×64 for approximately (3.75 mm $\times$ 3.75 mm $\times$ 3.8 mm)

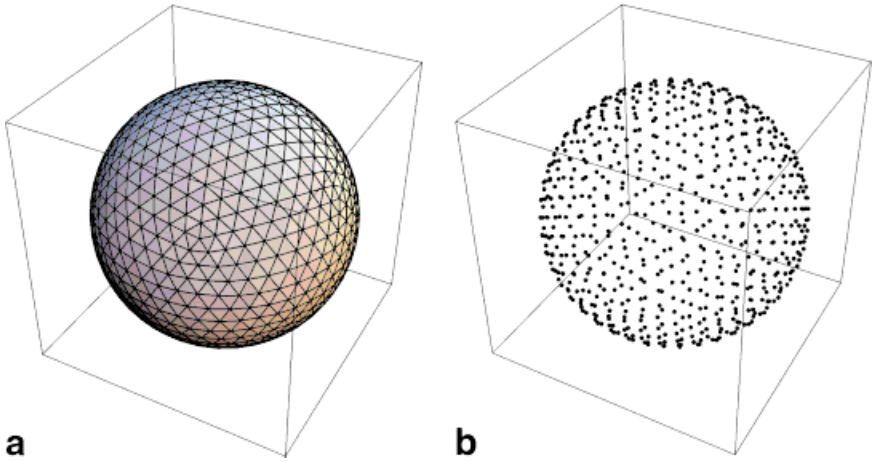

FIG. 4. Diffusion-encoding directions generated by the pulse sequence are spherical tessellations of an icosahedron (16) of user-specified order (shown here for clarity is fifth-order tesselation). **a:** Surface of measured diffusion directions. **b:** Diffusion-gradient directions (vertices in **a**). [Color figure can be viewed in the online issue, which is available at www.interscience.wiley.com.]

isotropic resolution, TR = 2700 ms, TE = 52 ms. The diffusion parameters were: diffusion gradient duration $\delta = 20$ ms, stimulated-echo mixing time TM = 200 ms, and $b \approx 3000$ s/mm^2, and 43 diffusion directions determined by the icosahedral tesselations of a sphere (16). Twenty averages at each diffusion direction were collected to ensure high signal-to-noise, and resulted in a total scan time of ≈34 min. A more clinically reasonable implementation of this sequence currently used at our institution utilizes 43 diffusion-encoding angles with only five averages, and only takes ≈9 min. An important consideration in the reconstruction of diffusion-weighted spiral images is the effect caused by phase variations. Pulsed-gradient experiments are susceptible to phase variations caused by eddy currents induced in the scanner by the pulsed fields (25), and can cause strong phase variations between images and subsequent strong spatial magnitude variations. However, averaging of the *magnitude* images from multiple excitations of the same diffusion encoding greatly reduces these artifacts (26). This averaging does not correct for eddy current distortions, however, and future work will focus on their reduction.

RESULTS

In Fig. 5 are shown the results of the spherical diffusion variance $\mathcal{V}$ computation along with those from the relative anisotropy index (27) as determined from the diffusion tensor, which is computated by fitting the full data from the six unknown diffusion components by linear regression, as in Ref. 6. The spherical diffusion variance image appears to show significantly more detail in the fiber structure, and is generally "cleaner." The arrows in Fig. 5 illustrate the important difference between the two methods of analysis. The images look similar in regions, such as the corpus callosum, in which the intravoxel fiber orientation is essentially unidirectional. However, in regions of crossed fibers, such as the corona radiata (highlighted by arrows), the diffusion tensor is a poor model for the local diffusion, and can result in an insensitivity to the anisotropy, as seen by the dark areas in the relative anisotropy map. The spherical diffusion variance, on the other hand, in quantifying deviations from a spherical surface that represents isotropic diffusion, is sensitive to deviations not well represented by the diffusion tensor. This is seen on the spherical diffusion variance map in Fig. 5, in which the corona radiata reappear as a region of strong diffusion variance. The reason for this improvement is clear from the angular distribution of the ADC shown in Fig. 6 for two voxels: one in the corpus callosum, the other in the corona radiata. Referring back to Fig. 3, the aligned fibers in the corpus callosum produce the characteristic "peanut" shape of anisotropic diffusion within a single-

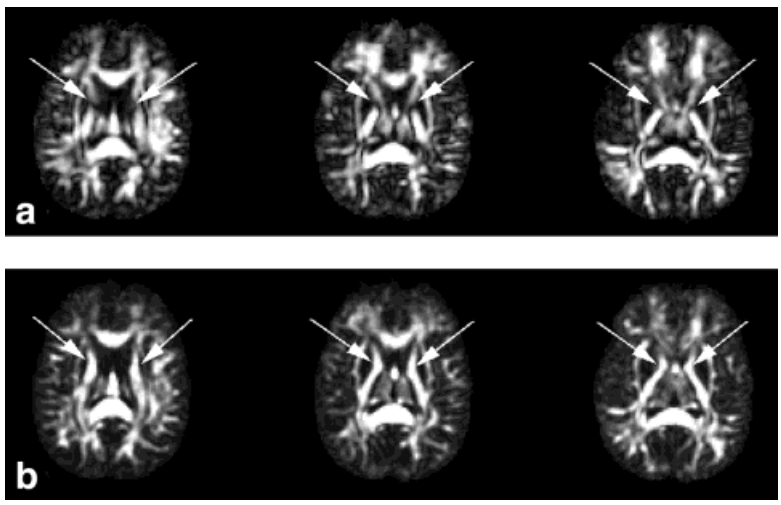

FIG. 5. Anisotropy measurements in three slices (left to right) from a spiral acquisition with 42 diffusion-encoding directions isotropically distributed on the surface of a sphere. The *b*-value was ≈3000 s/mm^2. Arrows point to regions where the diffusion tensor does not accurately predict diffusion anisotropy. **a:** Relative anisotropy index. **b:** Spherical diffusion variance.

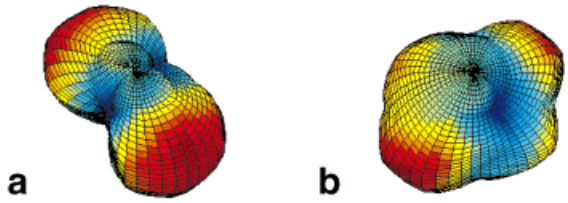

FIG. 6. Single-voxel measurements of the ADC as a function of the azimuthal and polar angles (θ, ϕ) from 42 measured gradient directions on the surface of a sphere. Surfaces were computed by interpolating the measured data onto a grid in (θ, ϕ). **a:** Corpus callosum. **b:** Corona radiata.

component voxel and are well characterized by the diffusion tensor. The shape of the radial local diffusion in the corona radiata, on the other hand, is similar to the crossed fiber simulation, in which the diffusion tensor produces spurious anisotropy measurements. These variations are present, however, in the spherical variance calculation. Close inspection of Fig. 5 reveals several such areas. Results from the other four subjects show similar patterns.

CONCLUSIONS

The local structure of the diffusion in voxels with multidirectional fibers can be quite complicated, and is not necessarily well characterized by a single diffusion tensor. It has been shown that diffusion anisotropy measured in high angular resolution diffusion experiments can be expressed using the variance of the ADC measurements, which we have termed the spherical diffusion variance. This method can reveal diffusion anisotropy in situations in which the diffusion tensor formalism fails to accurately reflect the local diffusion characteristics. Moreover, the calculation is very simple and is significantly less computationally intensive than those required to estimate the diffusion tensor, and much less so than those required to fit multiple tensors. The technique presented here is expected to be increasingly important for studies with high *b*-values in which multicomponent structure of the diffusion becomes more apparent, as seen in Fig. 1, but it has also proven useful at the lower *b*-values typically used in clinical studies ($b \approx 400$ s/mm^2). An obvious difficulty with our approach is the lack of any clear identification of "direction," such as afforded by the principal eigenvectors of the diffusion tensor. This is the price paid for looking at the magnitude of the deviations from isotropy. Future research should quantify these variations in order to better characterize the local diffusion characteristics.

ACKNOWLEDGMENTS

We thank Dr. Gary Glover at Stanford University for graciously providing the basic spiral pulse sequence and reconstruction software upon which our sequence was developed, Drs. Rick Buxton and Eric Wong for helpful discussions, and Dr. Van Wedeen for stimulating discussions on the importance of high angular resolution diffusion imaging.

REFERENCES

1. Carr HY, Purcell EM. Effects of diffusion on free precession in nuclear magnetic resonance experiments. Phys Rev 1954;94:630–638.
2. Hahn EL. Detection of sea-water motion by nuclear precession. J Geophys Res 1960;65:776.
3. Cooper RL, Chang DB, Young AC, Martin CJ, Ancker-Johnson B. Restricted diffusion in biophysical systems. Biophys J 1974;14:161.
4. Tanner JE. Transient diffusion in system partitioned by permeable barriers. Application to NMR measurements with a pulsed field gradient. J Chem Phys 1978;69:1748–1754.
5. Cotts RM, Hoch MJR, Sun T, Marker JT. Pulsed field gradient stimulated echo methods for improved NMR diffusion measurements in heterogeneous systems. J Magn Reson 1989;83:252–266.
6. Basser PJ, Mattiello J, Le Bihan D. Estimation of the effective self-diffusion tensor from the NMR spin echo. J Magn Reson 1994;103:247–254.
7. Basser PJ, Mattiello J, Le Bihan D. MR diffusion tensor spectroscopy and imaging. Biophys J 1994;66:259–267.
8. Chenevert TL, Brunberg JA, Pipe JG. Anisotropic diffusion in human white matter: demonstration with MR techniques in vivo. Radiology 1990;177:401–405.
9. Doran M, Hajnal JV, Van Bruggen N, King MD, Young IR, Bydder G. Normal and abnormal human white matter tracts shown by MR imaging using directional diffusion weighted sequences. J Comput Assist Tomogr 1990;14:865–873.
10. Mori S, Crain BJ, Chacko VP, van Zijl PC. Three-dimensional tracking of axonal projections in the brain by magnetic resonance imaging. Ann Neurol 1999;45:265–169.
11. Conturo TE, Lori NF, Cull TS, Akbudak E, Snyder AZ, Shimony JS, McKinstry RC, Burton H, Raichle ME. Tracking neuronal fiber pathways in the living human brain. Proc Natl Acad Sci USA 1999;96:10422–10427.
12. Basser P, Pajevic S, Pierpaoli C, Duda J, Aldroubi A. *In vivo* fiber tractography in human grain using diffusion tensor MRI (DT MRI) data. Magn Reson Med 2000;44:625–632
13. Pierpaoli C, Jezzard P, Basser PJ, Barnett A, DiChiro G. Diffusion tensor MR imaging of the human brain. Radiology 1996;201:637–648.
14. Basser PJ, Pierpaoli C. A simplified method to measure the diffusion tensor from seven MR images. Magn Reson Med 1998;39:928–934.
15. Pierpaoli C, Basser PJ. Toward a quantitative assessment of diffusion anisotropy. Magn Reson Med 1996;36:893–906.
16. Tuch DS, Weisskoff RM, Belliveau JW, Wedeen VJ. High angular resolution diffusion imaging of the human brain. In: Proceedings of the 7th Annual Meeting of ISMRM, Philadelphia, 1999. p 321.
17. Wedeen VJ, Reese TG, Tuch DS, Weigel MR, Dou J-G, Weiskoff RM, Chesler D. Mapping fiber orientation spectra in cerebral white matter with Fourier transform diffusion MRI. In: Proceedings of the 8th Annual Meeting of ISMRM, Denver, 2000. p 82.
18. Cory DG, Garroway AN. Measurement of translational displacement probabilities by NMR: an indicator of compartmentation. Magn Reson Med 1990;14:435.
19. Hsu EW, Mori S. Analytical expressions for the NMR apparent diffusion coefficients in an anisotropic system and a simplified method for determining fiber orientation. Magn Reson Med 1995;34:194–200.
20. Glover GH. Simple analytic spiral k-space algorithm. Magn Reson Med 1999;42:412–415.
21. Meyer CH, Hu BS, Nishimura DG, Macovski A. Fast spiral coronary artery imaging. Magn Reson Med 1992;28:202–213.
22. Tanner JE. Use of the stimulated echo in NMR diffusion studies. J Chem Phys 1970;52:2523–2526.
23. Merboldt K-D, Hanicke W, Frahm J. Self-diffusion NMR imaging using stimulated echoes. J Magn Reson 1995;64:479–486.
24. Cox RW, Jesmanowicz A, Hyde JS. A program for the analysis for functional magnetic resonance imaging data. Computer Vision and Graphics, 1996. Available at http://varda.biophysics.mcw.edu.
25. Morich MA, Lampman DA, Dannels WR, Goldie FTD. Exact temporal eddy current compensation in magnetic resonance imaging systems. IEEE Trans Med Imaging 1988;7:247–254.
26. Trouard TP, Theilman RJ, Altbach MI, Gmitro AF. High resolution diffusion imaging with DIFRAD-FSE (diffusion-weighted radial acquisition of data with fast spin-echo) MRI. Magn Reson Med 1999;42:11–18.
27. Basser PJ, Pierpaoli C. Microstructural and physiological features of tissues elucidated by quantitative diffusion tensor MRI. J Magn Reson B 1996;111:209–219.